RESEARCH ARTICLE | MAY 02 2023

Settling behavior of polydisperse droplets in homogeneous isotropic turbulence ⊘

Zhu Hang-Yu (朱航宇) ; Pan Chong (潘翀) ✉ ; Lian Huan (连欢) ✉

Check for updates

View Online   Export Citation

08 April 2024 03:27:00

Physics of Fluids

Special Topic:

John Michael Dealy (1937-2024): Celebrating His Life
Guest Editors: Alan Jeffrey Giacomin and Savvas G. Hatzikiriakos

Submit Today!

AIP Publishing

AIP Publishing

Settling behavior of polydisperse droplets in homogeneous isotropic turbulence

View Online   Export Citation   CrossMark

Hang-Yu Zhu (朱航宇),[1,2,3] (iD) Chong Pan (潘翀),[2,4,a] (iD) and Huan Lian (连欢)[1,a] (iD)

AFFILIATIONS

[1]State Key Laboratory of High Temperature Gas Dynamics, Institute of Mechanics, Chinese Academy of Sciences, Beijing 100190, China

[2]Fluid Mechanics Key Laboratory of Education Ministry, Beihang University, Beijing 100191, China

[3]Center for Complex Flows and Soft Matter Research and Department of Mechanics and Aerospace Engineering, Southern University of Science and Technology, Shenzhen 518055, China

[4]Aircraft and Propulsion Laboratory, Ningbo Institute of Technology, Beihang University, Ningbo 315800, China

[a]Authors to whom correspondence should be addressed: panchong@buaa.edu.cn and hlian@imech.ac.cn

ABSTRACT

The settling behavior of polydisperse droplets in homogeneous and isotropic turbulence was measured by an ultra-high-resolution two-dimensional Particle Image Velocimetry. The aim of the present study is to provide new insight on the dependence of multi-scale particle settling behavior on characteristic parameters of two-phase turbulent flow via a sophisticate conditional analysis. The relative settling strength (defined as the ratio of mean droplet settling velocity to root mean square velocity of turbulence), whose effect on droplet settling behavior is of the primary interest, ranges as $Sv_L = 0.5$–2.0. The turbulence Taylor Reynolds number is $Re_\lambda = 200$–300, and the droplet Stokes number is $St_p = 0.1$–10. Voronoï analysis is performed to obtain the concentration field of discrete droplets from particle images. Particle structures including clusters or voids are detected, and the droplet settling velocities corresponding to various probing conditions, such as St_p, local particle concentration, and size of particle structures, were then analyzed. For the present configuration (droplet net sedimentation), there is a non-monotonic dependency of the settling velocity on local particle concentration. The negative correlation between them occurs in the moderate-concentration sub-regime and is insensitive to the variation of Sv_L, in which individual droplets interact with turbulent flow independently. It can be well explained by the commonly invoked preferential sweeping mechanisms. On the other hand, the dense-concentration regime, in which droplets prefer to accumulate into clusters, presents a positive correlation; namely, the conditional-averaged settling velocity decreases with the increase in local particle concentration. In this sub-regime, it is not the scale of single particles but the scale of particle clusters and the relative strength of turbulence (measured by Sv_L) that jointly determines the droplet settling behavior. Such a process, to our knowledge, is consistent with the so-called multi-scale preferential sweeping effect.

I. INTRODUCTION

The motion of inertial particles settling in turbulence under the effect of gravity is widely encountered in environmental phenomena and engineering applications, including rainfall in atmospheric turbulence, pollen dispersion by wind, sediment transport, spray dynamics in combustion chamber, etc.[1–4] Particle settling is one of the most important issues in the studies of two-phase turbulence. For the purpose of modeling and controlling particle dynamics, it is desirable to characterize the settling behavior of discrete particles as well as to understand the underlying mechanisms.

When falling through turbulence, inertial particles are affected by turbulent motions with a wide range of scales. In general, the interaction between continuous and dispersed phases is governed by a set of dimensionless parameters, such as particle Stokes number St_p (the ratio of the particle response time τ_p to Kolmogorov timescale τ_η of turbulence), turbulence Reynolds number of turbulence $Re_\lambda = \lambda u_{rms}/\nu$ (with λ the transverse Taylor microscale, u_{rms} the turbulence fluctuation intensity, and ν the kinematic viscosity), and particle Reynolds number $Re_p = d_p U_{slip}/\nu$ (with d_p the particle diameter and U_{slip} the particle slip velocity).[5,6] The effect of gravity brings additional complexity to particle–turbulence interaction via a dimensionless parameter, i.e., the relative settling strength Sv (or called the settling parameter[7,8] and the Rouse number[9,10]), which is defined as the ratio of particle settling velocity to characteristic turbulent velocity.

Owing to the so-called preferential particle concentration effect, inertial particles are prone to accumulate in low-vorticity/high-strain regions,[11] leading to a non-homogeneity of particle distribution.[9,12] Another important issue is that turbulent structures are apt to alter the settling behavior of dispersed particles.[13–15] The pioneering work of Maxey[11] explored the gravitational settling of aerosol particles in a Gaussian random flow field by numerical simulations. It was found that the presence of turbulence enhanced the average settling velocity of inertial particles. This finding was supported by several direct numerical simulations (DNS)[16–19] and experimental measurements.[7,8,20] A well-accepted explanation for the settling enhancement phenomenon, as proposed by Maxey,[11] is the preferential sweeping effect; namely, inertial particles are prone to accumulate in the downward flow region of turbulent eddies under the effect of gravitational settling. A direct inference of this effect is that there is unbalanced concentration of ascending or descending particles in the downwash- or upwash-side of turbulent eddies.

In addition to the particle settling enhancement, the reduction of the averaged particle settling velocity in turbulence has also been reported by several studies.[21–23] Nielsen[21] termed this phenomenon as the loitering effect, i.e., heavy descending particles prefer to spend more time in updrifts of turbulence than in downdrifts. Good et al.[7] observed the loitering effect in the case of large particle Stokes number St_p (≈ 10) and attributed it to the nonlinear drag acting on heavy particles. However, this observation seems to conflict with several following studies. For instance, Petersen et al.[8] failed to observe the loitering effect for high-inertia particles in their experiments. Moreover, both the numerical studies of Rosa et al.[17] and Baker et al.[24] suggested that the nonlinear drag was not a determining factor for the occurrence of the loitering effect.

To clarify the exact condition for the appearance of particle settling enhancement, several studies have focused on the influence of St_p, Sv, and Re_λ on the particle settling behavior. Among them, Good et al.[7] showed that the settling velocity is enhanced by turbulence in the case of small Sv and is reduced by turbulence if both Sv and St_p are large. Petersen et al.[8] demonstrated that the settling enhancement reaches the maximum when both St_p and Sv are close to unity. Mora et al.[10] experimentally found that the settling enhancement (or suppression) occurs when Sv is below (or above) a critical value, and this critical Sv decreases with the increase in Re_λ. They also reported that turbulence enhances particle settling at moderate Re_λ but suppresses particle settling at higher Re_λ. It is noted that several of these studies lead to conflicting conclusions. One of the possible reasons, to our knowledge, might be the lack of the consensus, on which scales of turbulence are the most relevant for the complex process of particle settling.

Wang and Maxey[16] argued that the particle settling behavior may be only affected by a limited range of scales of turbulent motions. Concretely, the enhancement of the particle settling velocity was found to depend on u_{rms} that is mainly contributed by large-scale turbulent motions.[16] Such an argument is consistent with the studies of Rosa et al.[17] and Berk and Coletti,[25] who reported a positive correlation between the level of particle settling enhancement and u_{rms}. Nevertheless, the experiments of Petersen et al.[8] showed that the particle settling enhancement increases with St_p. This implies that it is the small-scale components of turbulence motions (with timescale of τ_η) that play a dominant role. On the other hand, Yang and Lei,[26] Good

et al.,[7] and Mora et al.[10] suggested that since the particle settling velocity depends on both u_{rms} and St_p, a mixed length scale of $\tau_\eta u_{rms}$ seems to be a more relevant parameter.

Considering the multi-scale nature of turbulent motions, it is unlikely that only one scale of turbulent motions is responsible for the particle settling behavior. Instead, the presence of the so-called preferential particle concentration, which states that particles present multi-scale spatial distribution with a wide spectrum of local particle concentration,[9,20,27] might offer an alternative explanation. The justification is that particles clusters with various scales are preferentially sampled by turbulent coherent motions with compatible scales.[8,9,24,28] Therefore, it is reasonable to expect that particles in the same cluster might present similar settling behavior. In other words, the scales of groups of particles with spatial and kinematic coherence might be a determining factor. In fact, Tom and Bragg[29] proposed a mechanism of multi-scale preferential sweeping, according to which a wide range of scales of turbulent motions can enhance the particle settling, and the higher St_p or the larger Sv, the larger scales of turbulent motions that contribute to the settling enhancement. Nevertheless, quantitative evidence to support this multi-scale preferential sweeping effect is still lacking.

With this background, the present study focuses on an experimental attempt on the multi-scale settling behavior of droplets in homogeneous and isotropic turbulence (HIT). Key physical factors, including polydispersity,[30,31] gravitational settling,[13,18,32,33] and hydrodynamic interaction,[34,35] which cannot be fully resolved by the state-of-the-art numerical algorithms,[5,6] are implicitly embedded in the present experiment. The studied parameter space is $Sv_L = \bar{u}_{p2}/u_{f,rms}$ = 0.5–2.0 ($\bar{u}_{p2}$ is the mean settling speed of droplets and $u_{f,rms}$ is the root mean square of the fluctuating velocity of turbulence phase), $St_p = 10^{-1}–10^1$, and $Re_\lambda = 200–300$. This work is an extension of our previous one.[36] In that work, we explored the coherency and intermittency of the settling motions of polydisperse droplets under the effect of turbulence. The effect of St_p and Sv_L on the spatial velocity correlations (SVCs) and relative velocities (RVs) of droplets in HIT, which was produced by a turbulence box, was experimentally studied. It was found that near the dissipation range, the balance between the path-history effect due to particle inertia and the action of turbulent coherent motions makes the velocity statistics of inertial droplets, including the SVCs, energy distributions, and particle RVs and their intermittency, to present a nearly scale-independent behavior. This finding has practical implications for modeling and predicting inter-particle collisions in two-phase turbulence. Nevertheless, the effect of the preferential particle concentration and preferential sweeping on the droplet settling behavior was not covered in that work.

The aim of the present study is to uncover the mist of the dependence of multi-scale particle settling behavior on characteristic parameters of two-phase turbulence flow. To achieve this goal, Voronoï analysis[9,27,37] is performed to obtain the concentration field of discrete droplets from particle images being obtained by two-dimensional (2D) Particle Image Velocimetry (PIV). Particle structures including clusters or voids (with relatively high or low local particle concentration) are detected, and the droplet settling velocity corresponding to various probing conditions, such as St_p, local particle concentration, and size of particle structures, is then analyzed. The present study reveals a non-monotonic dependence of droplet settling velocity on local particle concentration. Moreover, it is found that the effect of multi-scale preferential sweeping is responsible for the settling enhancement of
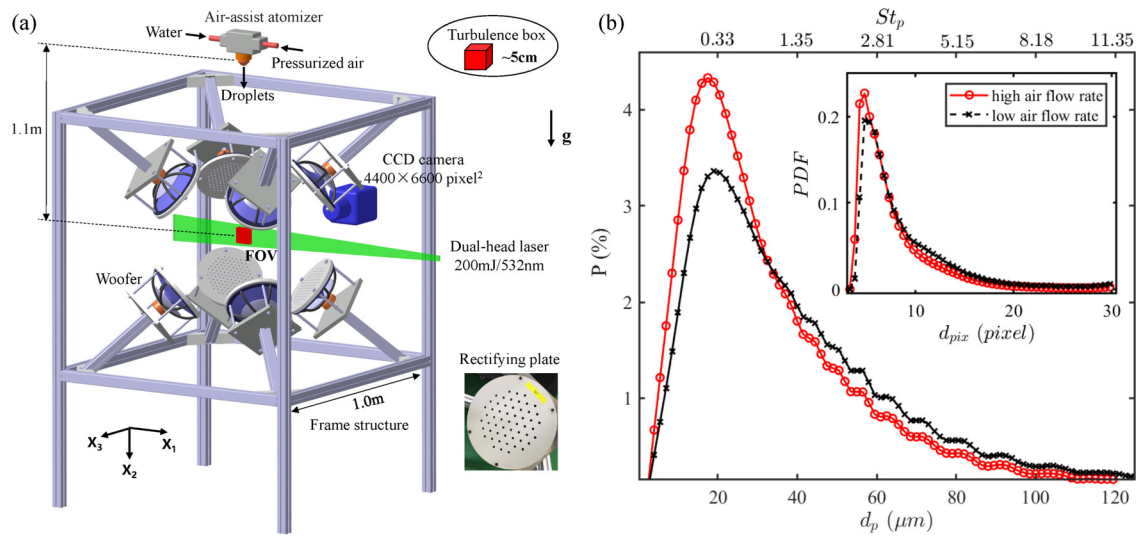
FIG. 1. (a) Schematic illustration of the experimental configuration, including the setup of the turbulence box, the droplet releasing device, and the 2D-PIV system. (b) The distribution of the physical diameter d_p of droplets being measured by a laser particle-size analyzer for two typical tested cases. The inset shows the distribution of the pixel diameter of droplets d_{pix} being measured from particle images.

dense droplets inside clusters. The underlying physics of such a scenario is quite different from the traditional concept of preferential sweeping, which applies for individual droplets with moderate local particle concentration.

The remainder of this paper is organized as follows. The experimental setup and the data processing method are introduced in Sec. II. Section III presents the experimental results in three parts. The manifestation of the preferential sweeping of particles is given in Sec. III A. Section III B deals with the dependence of the particle settling velocity on both local concentration and particle inertia. Section III C further analyzes the effect of the sizes of particle clusters and the relative settling strength on the particle settling velocity. Corresponding results in particle voids are also shown for a direct comparison. Concluding remarks are finally drawn in Sec. IV.

II. EXPERIMENTAL SETUP AND DATA PROCESSING METHOD

The experimental facility used for the generation of HIT has been described in detail in Zhu et al.[36] Here, we only provide a brief description to facilitate the related description. Following the previous study,[38] a so-called "turbulence box," which contains HIT without mean flow, was created in the converging region of an array of air jets. Specifically, as shown in Fig. 1(a), eight woofers were placed at the vertices of a cubic frame with a size of 1 m, each of which independently injected air jets through a perforated rectifier board into a common region. The interaction of these air jets produced the turbulent flows in the converged region. By adjusting the strength of each array of air jets, which can be achieved by changing the excitation voltage of each woofer, the turbulent flows at different Reynolds number can be produced. It has been checked by PIV measurements that the turbulence box has a size of approximately $5 \times 5 \times 5$ cm^3, in which the homogeneity and isotropy of the statistics of turbulent motions are well satisfying.[36] An ultra-high-resolution 2D PIV system was used to check the

quality of the turbulence box. This PIV system composes of a dual-head Nd:YAG laser (Beamtech, Vlite-200) with a wavelength of 532 nm and a maximum energy output of 200 mJ/pulse and a straddle-frame CCD camera (IMPERX ICL-B6640) with a sensor size of 4400×6600 pixels. In the present measurement, the sensor size has been cropped into 4400×4400 pixels. In the following, the horizontal direction and direction of gravity are denoted as x_1 and x_2, and the corresponding velocity components are u_1 and u_2, respectively. The subscripts f or p denote the quantities of fluid phase or particle phase, and the superscripts/subscripts C or V indicate the statistics conditioned inside particle clusters or voids.

Water droplets were released by a spay issued from an air-assist atomizer (Spraying Systems Co., Air Atom. 1/4-J 316SS), which was mounted 1.10 m above the turbulence box, as shown in Fig. 1(a). Four different cases with various characteristic parameters of both droplet motion and turbulent flow were tested individually. Table I summarizes the characteristic parameters of all four tested cases. The droplet settling velocity was adjusted by changing the air pressure and the water-flow rate in the atomizer, which slightly changed the distribution of the size of droplets in current experiment, as shown in Fig. 1(b). For all four tested cases, the relative settling strength Sv_L was 0.58, 0.85, 1.15, and 1.60. Meanwhile, the size of droplets, measured by a laser particle-size analyzer (LPSA, Dandong BetterSize Instruments LTd., BetterSize2000S), was in the range of $d_p = 10–120$ μm. The probability density functions of droplet size, i.e., PDF(d_p), are close to

TABLE I. Basic parameters for four tested cases.

Parameter	Case 1	Case 2	Case 3	Case 4
Sv_L	0.58	0.85	1.15	1.60
Re_λ	264	264	227	227
St_P	0.1–10	0.1–10	0.1–10	0.1–10

a lognormal profile [see Fig. 1(b)]. The droplet Stokes number St_p is estimated from τ_p/τ_η,[39,40] where τ_p is the particle relaxation time and τ_η is the Kolmogorov timescale of turbulence.[36] τ_p is calculated by $\tau_p = \rho_p d_p^2/18\nu\rho_f(1 + 0.15Re_p^{0.687})$, in which the water–air density ratio is $\rho_p/\rho_f = 775$, and the particle Reynolds number based on the slip velocity u_r is about $Re_p = d_p u_r/\nu \approx 1.0$ and the kinematic viscosity of air ν is 1.57×10^{-5} m²/s. In this experiment, the droplet Stokes number St_p ranges from $O(10^{-1})$ to $O(10^1)$, and its mean value is around 0.2–0.3 based on arithmetic mean diameter and 0.95–1.25 based on Sauter mean diameter.[38,41] It is noted that due to the polydisperse nature [see the raw particle image in Fig. 2(a), for instance], the effect of the size of droplets on particle settling behavior will be studied by partitioning the droplet size distribution in each case; therefore, the slight difference in PDF (d_p) among four tested cases is not concerned anymore.

The turbulence Reynolds number was changed by adjusting the strength of the air jets. Re_λ values in the present experiment are 264 (for case 1 and case 2) and 227 (for case 3 and case 4), and the corresponding Kolmogorov length scales are $\eta = 0.209$ and 0.226 mm, respectively, which are noticeably larger than d_p. The corresponding Kolmogorov velocity scales used for the normalization of the settling velocity are $u_\eta = 0.075$ and 0.068 m/s for $Re_\lambda = 264$ and 227, respectively. Since Sv_L is indirectly related to Re_λ, the effect of Re_λ will not be separately discussed in the following.

In each case, 2D velocity fields of droplet phase in the symmetric vertical $x_1 - x_2$ plane of the turbulence box were measured by the 2D PIV system. In the PIV measurement, a field of view (FOV) of 53.5×53.5 mm² was imaged by a CCD camera through a 180 mm lens. The resulting magnification was around 12.2 μm/pixel with the resolution of 4400×4400 pixels in the CCD camera. The droplet volume fraction in the turbulence box is $\Phi_V = O(10^{-6})$, close to the one-way coupling regime;[42] therefore, the feedback effect of the droplet motions on the turbulence characteristics is estimated to be rather small. Owing to the dilute volume fraction, individual droplets can be detected from the recorded particle images [see Fig. 2(a)] by conventional particle

identification algorithm being widely used in particle tracking velocimetry (PTV).[43] In addition, the ultra-high resolution of the present PIV measurement enables an estimation of the pixel sizes d_{pix} of each detected droplets from the particle images. As shown in the inset of Fig. 1(b), most of d_{pix} ranges from 3.0 pixels to 30 pixels, and its distribution, i.e., PDF(d_{pix}), is similar to the distribution of the physical diameter of droplets, i.e., PDF(d_p), being measured by LPSA. In this sense, it is reasonable to map the pixel size of one droplet to its physical size. As will be shown later, although such an image-based estimation on d_p is rough, it fascinates the following study on the effect of St_p on particle settling behavior in the circumstance of polydispersity. For each case, 1800 instantaneous snapshots were captured at a sampling rate of 1 Hz, leading to an ensemble of $O(10^7)$ individual droplets, which is sufficient for the convergence of the droplet velocity and concentration statistics to be presented later. For each detected droplet, its instantaneous velocity was calculated by an in-house PIV–PTV algorithm.[39] The uncertainty of the velocity measurement is approximately 1 %.[9,36]

Owing to the particular configuration of the experiment facility, the droplets generally present a decelerating trend when settling through the turbulence box; namely, the time-averaged settling velocity $\bar{u}_{p2}(x_1, x_2)$ decreases by approximately 30% within the vertical FOV of $\Delta x_2 = 53.5$ mm. The previous studies[41,44] reported a similar deceleration of the mean settling velocity of droplets injected by a spray. To isolate the settling behavior associated with the turbulence effect from the mean settling trend, the fluctuating velocity components, i.e., $\boldsymbol{u}'_p(x, y, t) = \boldsymbol{u}_p(x, y, t) - \bar{\boldsymbol{u}}_p(x, y)$ with $\bar{\boldsymbol{u}}_p(x, y)$ the local time-averaged droplet velocity at the spatial position of (x, y), are focused in the following.

The method of Voronoï diagram[27] is used to obtain the droplet concentration field. As shown in Fig. 2(b), the spatial domain of a set of discrete droplets is uniquely divided into a series of non-overlapped Voronoï cells, each of which is occupied by one individual droplet. Following the previous studies,[8,9,45] we use the normalized Voronoï area, i.e.,
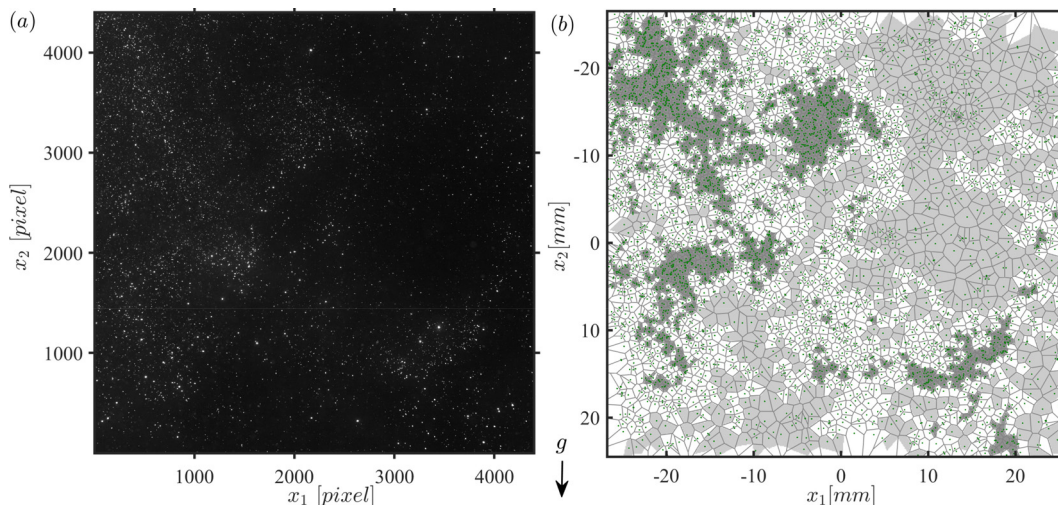
FIG. 2. (a) An instantaneous snapshot of raw particle images and (b) the corresponding Voronoï diagrams of the spatial distribution of detected droplets (as denoted by the green dots) for the case of $Sv_L = 0.58$. The dark and light patches in the background of (b) indicate the clusters and voids detected in this snapshot, respectively, and each connected group of cells represents an individual particle cluster or void.

$$\gamma(x, y, t) = A(x, y, t)/\bar{A}(x, y) \quad (1)$$

with $\bar{A}(x, y)$ the time-averaged area of the Voronoï cell area at (x, y), to eliminate the inhomogeneity of the time-averaged spatial distribution of droplets. It has been checked that the aforementioned treatments make the PDFs of γ and $\boldsymbol{u}_p$ independent of the spatial position; therefore, the statistics of γ and $\boldsymbol{u}_p$ to be presented later are counted in the whole measurement FOV.

The inverse of γ serves as a measure of local concentration of particles associated with the turbulence effect. Following Monchaux et al.,[27] the profiles of PDF(γ) are compared with that of the random Poisson process (RPP) to determine the clustering feature of discrete particles in turbulent flows. As shown in Fig. 3(a), there are two intersections between these two curves. The left intersection γ_C is regarded as the upper bound for those Voronoï cells belonging to particle clusters, while the right one γ_V is the lower bound corresponding to particle voids.[27] For the presently studied four cases, the intersections are $\gamma_C \approx 0.65$ and $\gamma_C \approx 2.1$, both of which are quasi-independent of both Sv_L and Re_λ. Those connecting cells with $\gamma < \gamma_C$ or $\gamma > \gamma_V$ are then assembled as one particle cluster or particle void [see the dark and light patches in Fig. 2(b) for illustration]. The sizes of clusters and voids, i.e., A_C and A_V, represented by the area of individual connected patches shown in Fig. 2(b), can then be calculated. For the purpose of accurately determining the size of particle structures, those particle clusters/voids that intersect with the boundary of FOV are excluded from the statistic ensemble in the following analysis. Additionally, those particle structures containing less than three droplets are also eliminated. The distributions of A_C normalized by its mean value for all tested cases are summarized in Fig. 3(b). A self-similar scaling of $PDF(A_C) \sim A_C^{-2}$ is clearly seen, consistent with the previous studies.[24,45]

III. EXPERIMENTAL RESULTS

A. Manifestation of multi-scale preferential sweeping

Figure 4 illustrates two typical snapshots of the spatial distribution and velocity vectors of droplets for two cases of $Sv_L = 0.58$ [Fig. 4(a), the same snapshot as Fig. 2(b)] and $Sv_L = 1.60$ [Fig. 4(b)]. In Fig. 4,
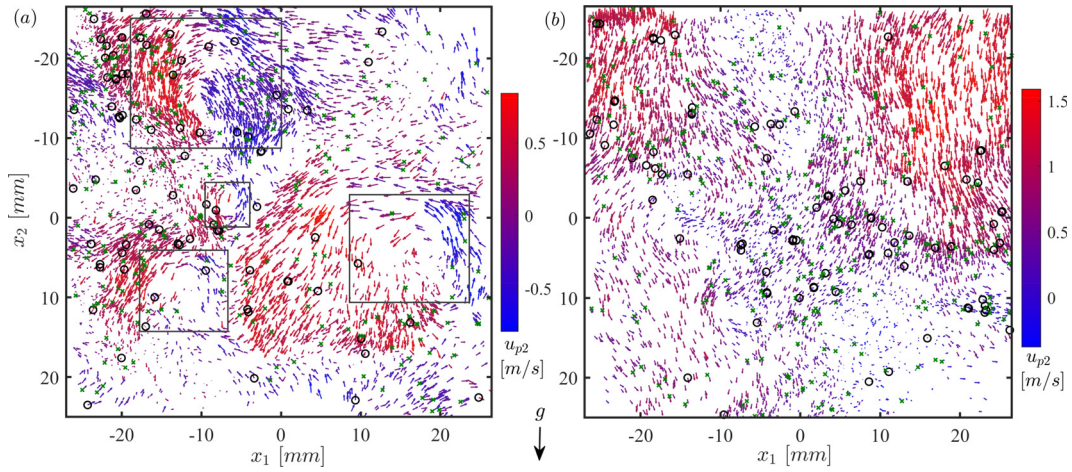
the velocity vectors of droplets with strong descending and ascending motions are colored in red and blue, respectively; meanwhile, two groups of droplets with different degree of inertia, i.e., $St_p = 3.2 \pm 0.4$ and $St_p = 0.6 \pm 0.05$, are highlighted by black circles and green crosses, respectively. Since two sub-figures present a distinct difference in the particle distribution pattern, they will be described separately.

Figure 4(a) leads to several interesting observations as follows. First, there is a strong spatial coherence between particle clusters and the periphery of turbulence vortices. The particle clusters can be seen from the groups of small gray Voronoï cells shown in Fig. 2(b); meanwhile, the existence of turbulence vortices can be inferred by the swirling motions in the vector plot of $\boldsymbol{u}_p$ (being highlighted by four gray rectangles) in Fig. 4(a). As shown in Fig. 3(b), the distribution of the sizes of particle clusters, i.e., PDF(A_C), of all four tested cases presents a power law with an index of -2 in a wide scale range. Such a multi-scale preferential concentration[28] suggests that the multi-scale nature of particle clusters might be related to multi-scale self-similar turbulent structures.[9,27,28] Second, compared to larger droplets [those indicated by black circles in Fig. 4(a)], smaller ones [green crosses in Fig. 4(a)] have less spatial coherence with turbulent vortices. Third, clusters of descending droplets (red vectors with $u_{p2} > 0$) and ascending ones (blue vectors with $u_{p2} < 0$) prefer to reside on the downwash side and upwash side of turbulence vortices, respectively. The number of descending droplets is considerably larger than that of the ascending ones. The imbalance between them becomes more prominent for large-scale turbulence vortices. This observation indicates the presence of the effect of multi-scale preferential sweeping.[29] Finally, Fig. 4(a) shows that droplets in the same cluster have similar $\boldsymbol{u}_p$. Therefore, it can be inferred that one of the dominant factors that affect the droplet settling behavior might be the particle concentration. Such an inference will be quantified by the following analysis on conditional statistics of the droplet settling velocity.

As shown in Fig. 4(b), the settling behavior and spatial distribution of droplets in the $Sv_L = 1.60$ case differ from that in the $Sv_L = 0.58$ case [Fig. 4(a)]. Specifically, for $Sv_L = 1.60$, nearly no swirling motions of droplets are seen, and their spatial distribution is more uniform.
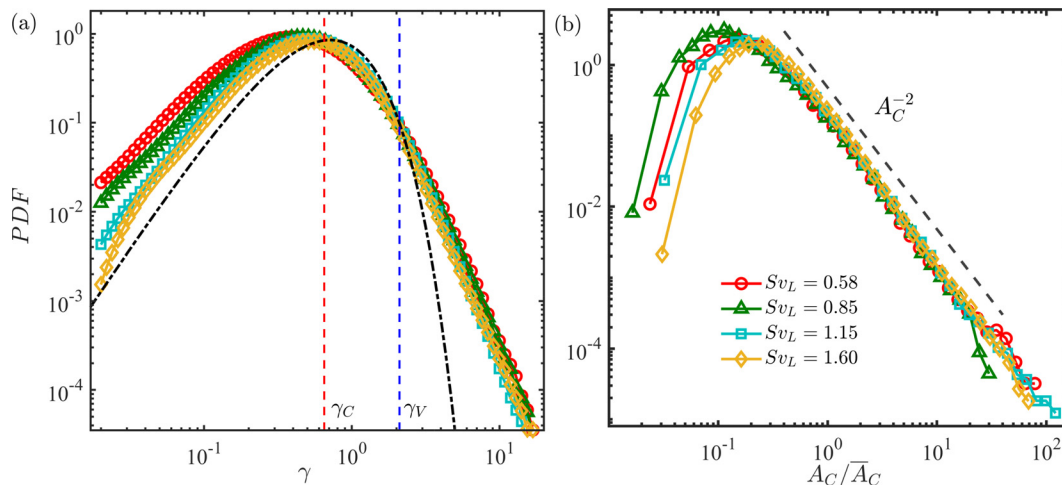
FIG. 3. (a) PDFs of dimensionless Voronoï cell area γ for different Sv_L cases. The PDF for RPP is shown as a black dash-dotted line, whose two intersections with the γ-PDF profiles yield the thresholds γ_C (= 0.65) and γ_V (= 2.1) for clusters and voids, respectively. (b) PDFs of cluster area A_C normalized by its respective mean value. The dashed line denotes the scaling of A_C^{-2} to show self-similarity of the droplet clusters.

FIG. 4. Instantaneous snapshot of velocity vectors of individual droplets in the cases of (a) $Sv_L = 0.58$ and (b) $Sv_L = 1.60$. Each velocity vector is colored by the magnitude of the vertical velocity component u_{p2}. Droplets with $St_p = 3.6(\pm 0.4)$ and $St_p = 0.6(\pm 0.05)$ are marked by large black circles and small green crosses, respectively. In (a), the swirling motions of droplets in the vector plot, being highlighted by four gray rectangles, infer the existence of turbulence vortices of different sizes.

This suggests a weakening trend of the effect of turbulent structures as Sv_L increases, which will be quantitatively demonstrated later.
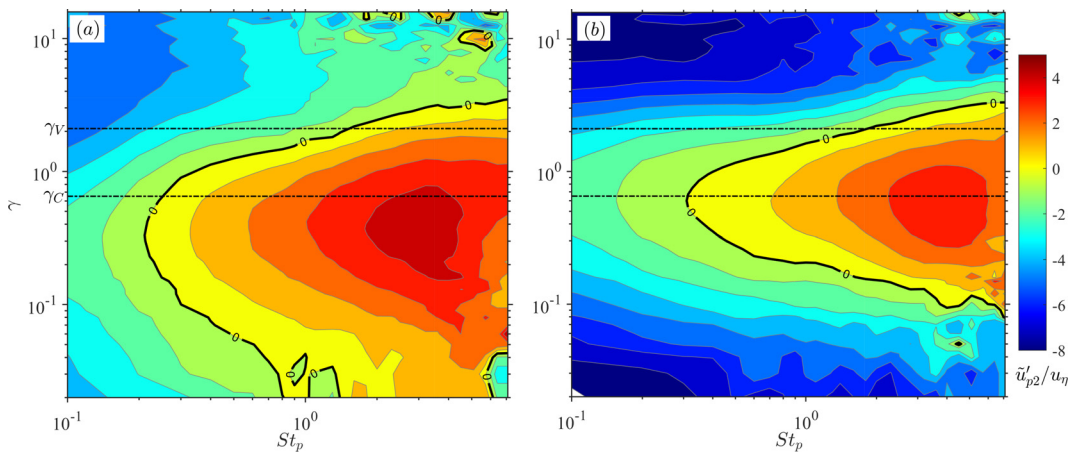
B. Settling velocity conditioned on γ and St_p

Given one droplet, its local concentration γ, diameter d_p, and settling velocity u'_{p2} can be obtained by the image processing method described in Sec. II. This enables a comprehensive study regarding the effect of both droplet concentration and particle inertia on the settling velocity.

Figure 5 shows the conditional-averaged vertical fluctuating velocity components $\tilde{u}'_{p2}/u_\eta$ of all droplet ensemble conditioned on γ and St_p for two cases of $Sv_L = 0.58$ and 1.60. Such a plot provides an overview on the role of local particle concentration, particle inertia, as well as the relative strength of turbulence intensity (measured by the inverse of Sv_L), on the droplet settling behavior. The line of $\tilde{u}'_{p2} = 0$,

denoted as bold solid lines in Fig. 5, divides the $\gamma - St_p$ phase plane into two parts: one with settling enhancement (with $u'_{p2} > 0$) and the other with settling suppression (with $u'_{p2} < 0$). The non-monotonic dependence of $\tilde{u}'_{p2}$ on γ and St_p is seen from the map of $\tilde{u}'_{p2}(\gamma, St_p)$, with the peak value of $\tilde{u}'_{p2}$ appearing around $St_p = 3–4$ and below $\gamma = \gamma_C$. As Sv_L decreases, the settling-enhanced region (with $u'_{p2} > 0$) expands in the $\gamma - St_p$ plane, consistent with the idea that with the presence of stronger turbulence, the settling of droplets could be enhanced in a wider parameter space.[29]

The map of $\tilde{u}'_{p2}(\gamma, St_p)$ shown in Fig. 5 fails to convey the information on the appearance frequency of droplets subject to different γ or St_p conditions. To compensate this limitation, the joint PDFs (JPDF) of St_p and γ of those droplets that present significant settling enhancement (with $u'_{p2}/u_\eta > 2$) or settling suppression (with $u'_{p2}/u_\eta < -2$) are shown in Fig. 6. It has been checked that the observation to be presented in the following does not dependent on the

FIG. 5. Conditional-averaged settling velocity fluctuation $\tilde{u}'_{p2}/u_\eta$ of droplets conditioned on γ and St_p for two Sv_L cases: (a) $Sv_L = 0.58$ and (b) $Sv_L = 1.60$. The two dash-dotted straight lines indicate the threshold of γ for the identification of cluster and voids. The bold black lines highlight the contour of $\tilde{u}'_{p2} = 0$.
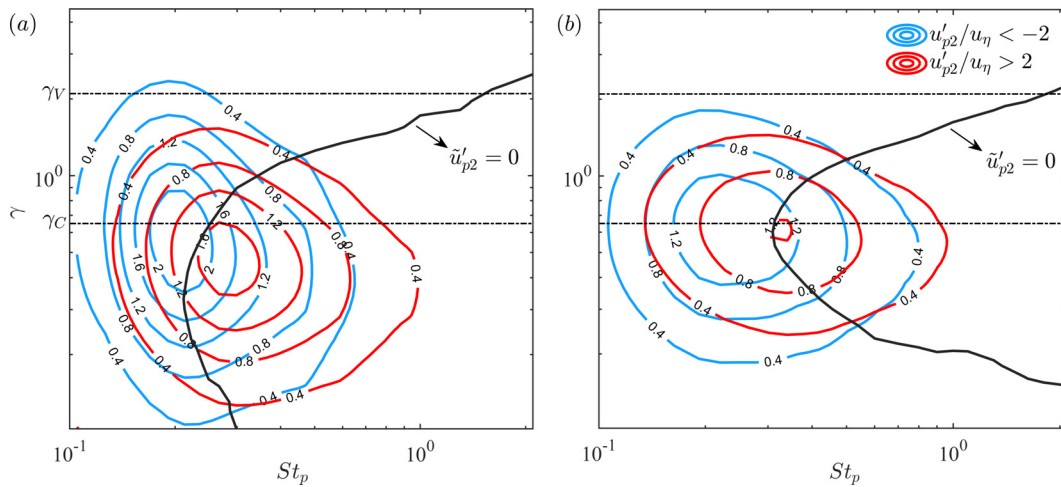
FIG. 6. Conditional joint PDFs of γ and St_p conditioned on fast- ($u'_{p2}/u_\eta > 2$) and slow-falling ($u'_{p2}/u_\eta < -2$) droplets for two Sv_L cases: (a) $Sv_L = 0.58$ and (b) $Sv_L = 1.60$. The bold black lines display the corresponding contours of $\tilde{u}'_{p2} = 0$ shown in Fig. 5.

exact magnitude of the threshold of u'_{p2}/u_η for settling enhancement or suppression. Similar to Figs. 4 and 5, only the cases of $Sv_L = 0.58$ and $Sv_L = 1.60$ are shown, and the contour of $\tilde{u}'_{p2} = 0$ is supplemented for reference. As shown in Fig. 6, the peaks in both two contours of JPDF(St_p, γ) of settling-enhanced and settling-suppressed droplets do not coincide with each other but are separated by the $\tilde{u}'_{p2} = 0$ line. Such a shift of the JPDF peaks evidences that settling-enhanced droplets usually have larger St_p and smaller γ, and vice versa for settling-suppressed droplets. This is consistent with the preferential sweeping effect being visualized in Fig. 4(a). For setting-enhanced droplets, a clear negative correlation between γ and St_p, which is indicated by the inclined ridge line of JPDF(γ, St_p), is seen in the case of $Sv_L = 0.58$. It suggests that fast-falling droplets with comparably higher inertia are prone to reside in high-concentration regions. Notably, a similar negative correlation between γ and St_p is absent in either setting-suppressed droplets or large Sv_L case (with $Sv_L = 1.60$).

To quantify the non-monotonic characteristics of droplet settling behavior, $\tilde{u}'_{p2}$ conditioned on either γ or St_p is further examined. The curves of $\tilde{u}'_{p2}(\gamma)$ or $\tilde{u}'_{p2}(St_p)$, as shown in Fig. 7, are obtained by integrating the map of $\tilde{u}'_{p2}(\gamma, St_p)$ along the axis of St_p or γ, respectively. For all the studied cases with different Sv_L, the corresponding curves present similar shape. Specifically, the curve of $\tilde{u}'_{p2}(\gamma)$ [shown in Fig. 7(a)] reaches a peak blow γ_C; meanwhile, $\tilde{u}'_{p2}$ increases with St_p till $St_p = 2$–4 [shown in Fig. 7(b)]. The decreasing trend of $\tilde{u}'_{p2}(St_p)$ in the range of $St_p \gtrsim 3.5$ can be attributed to the so-called loitering effect;[7,21,24] namely, particles with high inertia spend more time to cross upward-moving regions of flow when settling in turbulence. On the other hand, the lowest bound of St_p for $\tilde{u}'_{p2} > 0$ is seen to decrease with the decrease in Sv_L. This observation suggests that intenser turbulent fluctuation (with smaller Sv_L) might lead to stronger upwash/downwash induction, which, in turn, affects droplets with lower inertia.
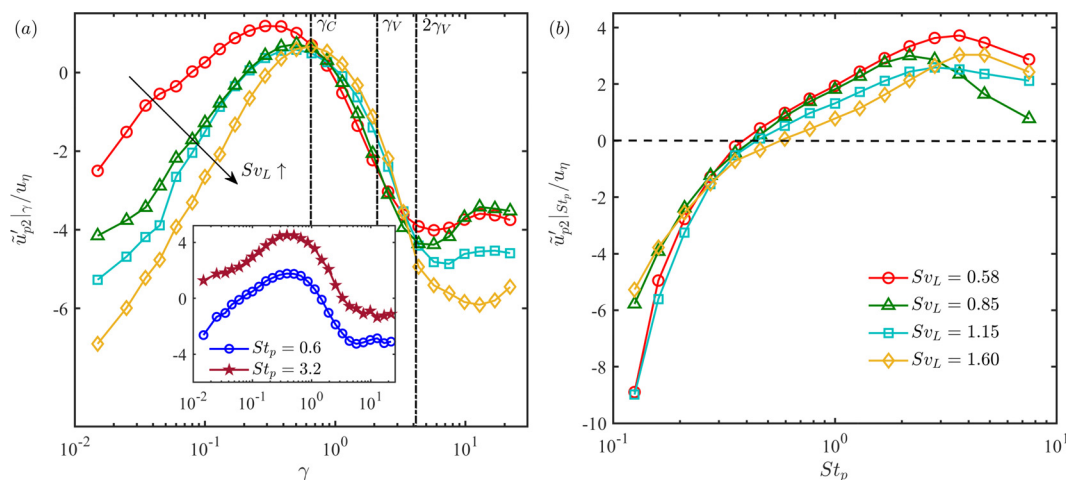
FIG. 7. Conditional-averaged settling velocity fluctuation $\tilde{u}'_{p2}/u_\eta$ as a function of (a) γ and (b) St_p for different Sv_L cases. The inset in (a) shows $\tilde{u}'_{p2}|_{St_p}/u_\eta$ as a function of γ conditioned on $St_p = 0.6$ or $St_p = 3.6$ for $Sv_L = 0.58$.

It also reminds us that the relative settling strength Sv_L should be taken into account when interpreting the inconsistency on the parameter dependency of particle settling enhancement in existing studies.[8,17,23,24]

Several studies have reported a monotonic increasing trend of particle settling velocity with respect to local particle concentration (measured by the inverse of γ).[8,14,20] To our knowledge, such a trend might be the part of the $\tilde{u}'_{p2}(\gamma)$ curve in the range of $\gamma_C < \gamma < 2\gamma_V$ [shown in Fig. 7(a)]. Below $\gamma = \gamma_C$, $\tilde{u}'_{p2}$ is seen to increase with the decrease in local particle concentration, while beyond $\gamma = 2\gamma_V$, the effect of γ on $\tilde{u}'_{p2}$ gradually saturates. On the other hand, $\tilde{u}'_{p2}$ decreases with the increase in Sv_L when $\gamma < \gamma_C$, but the effect of Sv_L on $\tilde{u}'_{p2}$ is insignificant in the range of $\gamma_C < \gamma < 2\gamma_V$. The latter observation indicates that for those droplets, which do not belong to any particle structures, their particle settling behavior might be independent from the relative settling strength. This infers a pure preferential sweeping process without the role of particle structures. In this sense, a self-similar settling behavior that is free from the effect of Sv_L might be expected in the range of $\gamma_C < \gamma < 2\gamma_V$. This issue is beyond the scope of the present study and deserves to be studied in the future. Finally, it is stressed that the non-monotonic dependence of $\tilde{u}'_{p2}$ on γ is insensitive to St_p, as can be seen by two curves of $\tilde{u}'_{p2}(\gamma)$ conditioned on St_p = 0.6 and 3.2 [shown in the inset of Fig. 7(a)]. Nevertheless, St_p, indeed, affects the magnitude of $\tilde{u}'_{p2}$.

It is noted that the aforementioned stated negative correlation between settling velocity and local particle concentration with $\gamma < \gamma_C$ has been reported by only a few existing studies. In the experimental study of a horizontal two-phase turbulent channel flow, Wang and Lam[46] observed the decrease in the settling velocity in high-particle-concentration regions and attributed it to the consequence of particle collisions. Momenifar and Bragg[47] reported that in homogeneous turbulence simulated by DNS, a similar negative dependence occurs in the cases of large Sv_L. The preferential sweeping effect,[11] which predicts the enhancement of particle settling in high-particle-concentration regions, fails to explain such a negative dependence. To our knowledge, the clustering of discrete particles into large-scale structures might offer an alternative explanation. The consideration is that when particle concentration is sufficiently high, it might not be individual particles but a group of collaborated ones that jointly interact with turbulent motions. Based on this consideration, the characteristics of droplet settling velocity conditioned on scales of particle clusters will be discussed in Sec. III C.

C. Settling velocity conditioned on scales of particle structures

The effect of the size of particle structures on the statistics of droplet settling velocity will be discussed. The whole ensemble of
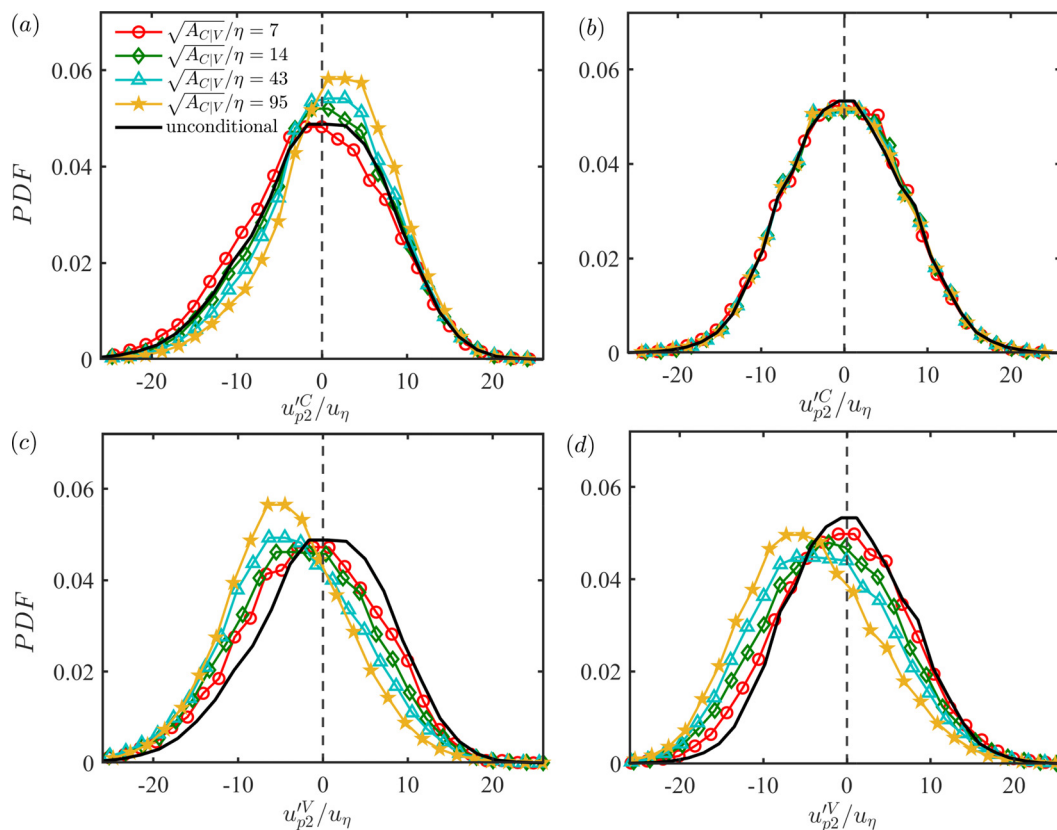
FIG. 8. PDFs of settling velocity fluctuation in clusters and voids of four values of area $A_{C|V}$ for two Sv_L cases: (a) u'^C_{p2}/u_η, $Sv_L = 0.58$; (b) u'^C_{p2}/u_η, $Sv_L = 1.60$; (c) u'^V_{p2}/u_η, $Sv_L = 0.58$; and (d) u'^V_{p2}/u_η, $Sv_L = 1.60$. The solid black lines show the corresponding unconditional results.

droplets inside clusters and voids is conditioned on the size of particle structures, i.e., A_C or A_V, that encompass the particular droplets, as shown in Fig. 2(b). The corresponding droplet settling velocity is denoted as $u_{p2}^{\prime C}$ or $u_{p2}^{\prime V}$ for particle clusters or voids, respectively.

The PDFs of $u_{p2}^{\prime C}$ in particle clusters with four typical sizes, i.e., $\sqrt{A_C}/\eta = 7$, 14, 43, and 95 in the cases of $Sv_L = 0.58$ and 1.60 are shown in Figs. 8(a) and 8(b), while the corresponding PDF($u_{p2}^{\prime V}$) profiles in particle voids with $\sqrt{A_V}/\eta = 7$, 14, 43, and 95 are plotted in Figs. 8(c) and 8(d). Figure 9 summarizes the statistics of $u_{p2}^{\prime C|V}$ as a function of $A_{C|V}$. The presented statistics in Fig. 9 are the conditional-averaged value $\tilde{u}_{p2}^{\prime C|V}$, the fraction of settling-enhanced examples in particle clusters or voids (with $u_{p2}^{\prime C|V} > 0$) and the skewness of PDF ($u_{p2}^{\prime C|V}$). Hereinafter, the results associated with particle clusters and voids will be discussed separately.

For the large Sv_L case (with $Sv_L = 1.60$), all the profiles of PDF ($u_{p2}^{\prime C}$) with different A_C [shown in Fig. 8(b)] present a symmetric Gaussian distribution, each of which collapses well with the PDF profile of the whole ensemble of $u_{p2}^{\prime C}$ (as indicated by the black solid curve in Fig. 8). For a wide range of A_C, the skewness of PDF($u_{p2}^{\prime C}$) is around zero, the fraction of ascending particles is equal to that of descending particles, and the conditional-averaged $\tilde{u}_{p2}^{\prime C|V}$ is close to zero. Such a A_C-independence indicates the absence of multi-scale preferential sweeping when the relative settling strength is large.

In contrast, the settling velocity in the small Sv_L cases is strongly dependent on A_C. Specifically, the profile of PDF($u_{p2}^{\prime C}$) for $Sv_L = 0.58$ is close to a symmetric Gaussian distribution when A_C is small, and it gradually skews toward the $u_{p2}^{\prime C} < 0$ direction with the increase in A_C. This leads to a persistent increase in both $\tilde{u}_{p2}^{\prime C}$ and the fraction of the droplets with $u_{p2}^{\prime C|V} > 0$, which is consistent with the visualization shown in Fig. 4(a); namely, droplets in large-scale clusters prefer to present distinct settling enhancement. As clearly shown in Fig. 9, such an increase trend gradually relaxes with the increase in Sv_L, and the A_C-independence is achieved when $Sv_L = 1.60$. Furthermore, it has been checked that for each tested Sv_L, the subsets of droplet ensembles with different St_p pose the same A_C-dependence or A_C-independence (not shown here for brevity).

Once accepting the idea that there is a scale correspondence between turbulent structures and particle clusters,[24,28,48] the aforementioned observation that droplets in clusters with various sizes have different settling behavior is actually a manifestation of the concept of multi-scale preferential sweeping,[29] which emphasizes the role of larger-scale turbulent structures on particle settling enhancement. In this sense, the dominant factor that affects the settling behavior in high-concentration regime is not the level of local particle concentration but the size of concentrated clusters. This might explain the non-monotonic dependence of $\tilde{u}_{p2}^{\prime}$ on γ being observed in Fig. 7(a). Additionally, Tom and Bragg[29] suggested that with the increase in Sv_L, the scales of turbulent motions being responsible for the settling
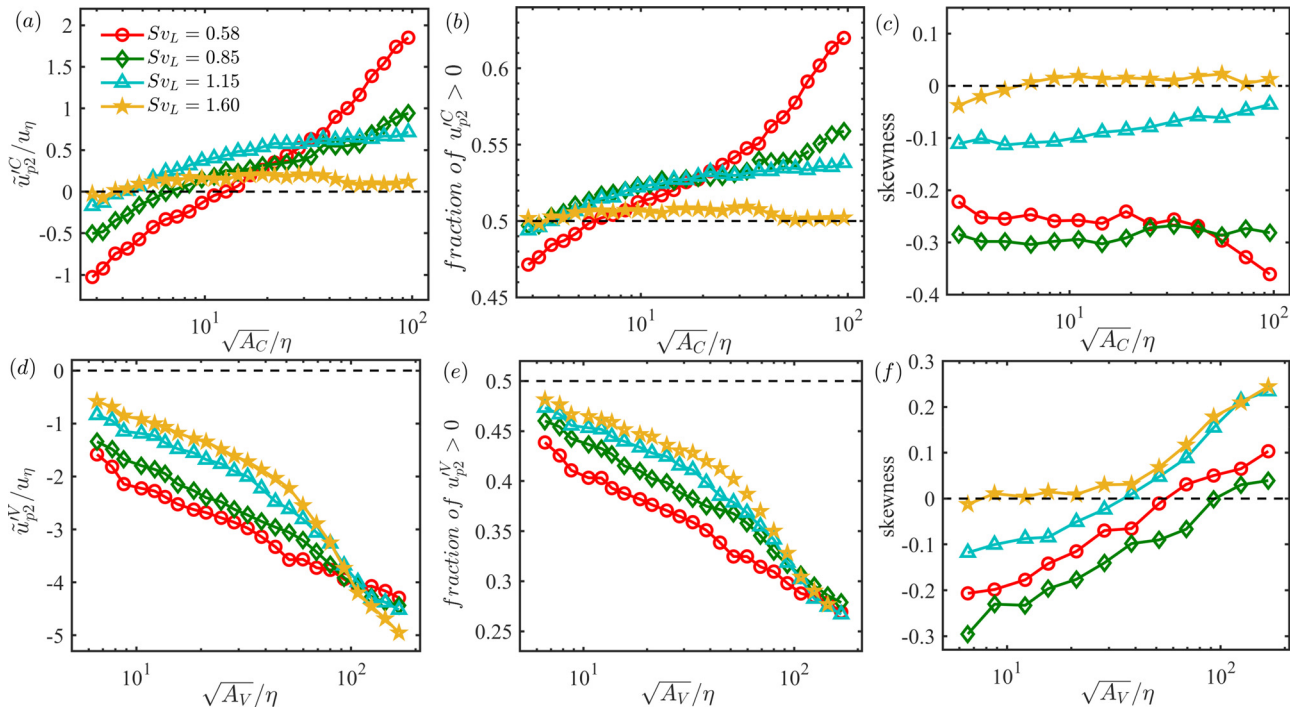
FIG. 9. Statistics of settling velocity fluctuation of droplets as a function of cluster (a)–(c) and void (d)–(f) sizes for different Sv_L cases: (a) and (d) mean settling velocity fluctuation $\tilde{u}_{p2}^{\prime C|V}/u_\eta$; (b) and (e) fraction of $u_{p2}^{\prime C|V} > 0$; and (c) and (f) skewness of PDF ($u_{p2}^{\prime C|V}$).

enhancement become larger. Such a viewpoint is supported by the observation in Fig. 9(a), i.e., the slope of the curve of $\tilde{u}_{p2}'^C(A_C)$ reduces with the increase in Sv_L, which evidences that small-scale clusters are incapable of contributing to the particle settling enhancement in the circumstance of large relative settling strength (or weak relative turbulence intensity).

Droplet settling behavior in voids [see Fig. 2(b)] differs from that in clusters in several aspects. First, droplets in voids have higher probability to present settling suppression, as can be seen from the right-skewed distribution of $u_{p2}'^V$ [in Figs. 8(c) and 8(d)] and the negative value of the conditional-averaged $\tilde{u}_{p2}'^V$ [shown in Figs. 9(d) and 9(e)]. The larger size voids have the higher fraction of settling-suppressed droplets being contained in voids and the smaller value of $\tilde{u}_{p2}'^V$. Second, unlike the relaxation of the A_C-dependence of $\tilde{u}_{p2}'^C$ in the large Sv_L case, the dependence of $\tilde{u}_{p2}'^V$ on A_V of voids remains in the whole Sv_L range being studied here. Third, except for extremely large voids (with $\sqrt{A_V}/\eta > 100$), the level of settling suppression (measured by $\tilde{u}_{p2}'^V$) decreases with increasing Sv_L. These observations jointly infer that the settling behavior of droplets in voids is less affected by multi-scale preferential sweeping. To our understanding, such an inference is reasonable, since due to low concentration in voids, individual droplets are unlikely to present a collaborate settling that are affected to multi-scale turbulent motions.

IV. DISCUSSION AND CONCLUSIONS

In our previous work,[36] we focused on the spatial velocity correlations and relative velocities of inertial droplets in turbulence, which has important implications for the understanding of the underlying physics of inter-particle collisions.[49,50] In the present work, another important issue, i.e., the variation of the settling velocity of particles under the effect of multi-scale turbulent structures, is addressed. Polydisperse water droplets were issued from a spay into a turbulence box in a sense of net sedimentation. The characteristic parameters of such a two-phase flow are $St_p = O(10^{-1})–O(10^1)$ and $Re_\lambda = 200–300$. The relative settling strength is a primary parameter whose effect on droplet settling behavior is of particular interest. It ranges as $Sv_L = 0.5–2.0$ in the present study. Since the ultra-high-resolution 2D PIV measurement enables a precise quantification of both geometries (particle size and local particle concentration) and kinematics (instantaneous 2D velocity) of individual droplets, the effect of St_p and γ can be studied by a comprehensive analysis on the conditional statistics of the fluctuating component of droplet settling velocity u_{p2}'.

In the present study, the settling enhancement of inertial droplets is found to reach maximum when the particle Stokes number is $St_p \sim O(10^0)$, consistent with the existing knowledge.[7,8] On the one hand, there is a non-monotonic dependency of droplet settling velocity on local particle concentration, which is clearly seen in the curves of the conditional-averaged $\tilde{u}_{p2}'$ conditioned on γ. It is in distinct contrast to several existing studies,[8,14,20] who only reported a monotonically increasing trend of particle settling velocity with respect to local particle concentration. The present study shows that such a trend occurs in the sub-regime of $\gamma_C < \gamma < 2\gamma_V$ (i.e., with moderate local particle concentration). On the other hand, a positive correlation between $\tilde{u}_{p2}'$ and γ is seen in the sub-regime of $\gamma < \gamma_C$ (with dense local particle concentration), while $\tilde{u}_{p2}'$ is free from γ in the sub-regime of $\gamma > 2\gamma_V$ (with dilute local particle concentration).

It is noted that previous studies[8,14,24] explain the negative correlation between $\tilde{u}_{p2}'$ and γ by the preferential sweeping effect,[11] which predicts a preferential accumulation of setting-enhanced particles along the downwash side of the periphery of turbulent eddies under the effect of gravity. The present study shows that the lower bound of such a negative-correlation sub-regime is beyond the threshold of particle clusters, i.e., $\gamma > \gamma_C$. This indicates that individual particles that do not belong to particle clusters are subject to a pure preferential sweeping effect. Combining with the observation that $\tilde{u}_{p2}'$ is quasi-independent from Sv_L in this sub-regime ($\gamma_C < \gamma < 2\gamma_V$), it is expected that a self-similarity of the settling behavior, which is invariant to the variation of turbulence intensity, can be seen for individual droplets with moderate local particle concentration. This issue deserves to be further studied in the future.

As for the sub-regime of $\gamma < \gamma_C$, the positive correlation between $\tilde{u}_{p2}'$ and γ is not a key to uncover the underlying physics in the circumstance of high particle concentration. Instead, the dominant factor becomes the size of particle clusters A_C and the relative settling strength Sv_L. For the case of small Sv_L, droplets in clusters with various sizes have different settling behavior. Namely, large-scale clusters are more likely to present particle settling enhancement. This leads to a positive correlation between $\tilde{u}_{p2}'^C$ and A_C. While in the scenario of large Sv_L, clusters with all scales contribute less to particle settling enhancement, a relaxation of the correlation between $\tilde{u}_{p2}'^C$ and A_c is observed. The reason is attributed to the decrease in the relative strength of turbulence with the increase in Sv_L, which, in turn, reduces the interaction between particle clusters and turbulent eddies. To our knowledge, the observed dependence of $\tilde{u}_{p2}'^C$ on A_C and Sv_L is a manifestation of multi-scale preferential sweeping,[29] which highlights the role of the interaction between particle clusters and turbulent eddies with comparable scales in the settling process of particles. Finally, the analysis on $u_{p2}'^V$ being conditioned inside voids demonstrates the absence of multi-scale preferential sweeping for those dilute droplets. This observation provides a counter evidence to suggest that the multi-scale preferential sweeping effect is noticeable only in multi-scale particle clusters.

To sum up, the present study provides solid experimental evidence to uncover the subtle difference between the traditional concept of preferential sweeping and the newly proposed multi-scale preferential sweeping. The former affects the settling behavior of isolated particles that are sampled by turbulent eddies as individual events, while the latter is more suitable to describe the interaction between particle clusters and turbulent eddies with comparable scales. It seems that the division between two effects is whether or not dense particles aggregate into clusters. For the moment, the cause-and-effect relationship between preferential sweeping and preferential particle concentration is unknown. Therefore, it is unclear whether or not preferential sweeping promotes local particle concentration and, thus, enhances settling speed of inertial particles. This issue deserves to be further studied by tracking the dynamics of individual particles or particle clusters in HIT. Nevertheless, the conflict on the condition for the appearance of particle settling enhancement in existing studies[7,8,10] can be interpreted from a new perspective by taking the level of local particle concentration into consideration.

AUTHOR DECLARATIONS

Conflict of Interest

The authors have no conflicts to disclose.

Author Contributions

Hangyu Zhu: Data curation (equal); Formal analysis (equal); Funding acquisition (equal); Investigation (lead); Methodology (equal); Writing – original draft (equal); Writing – review & editing (equal). **Chong Pan:** Conceptualization (equal); Formal analysis (equal); Funding acquisition (equal); Methodology (equal); Project administration (equal); Writing – original draft (equal); Writing – review & editing (equal). **Huan Lian:** Conceptualization (equal); Data curation (equal); Funding acquisition (equal); Methodology (supporting); Project administration (equal); Writing – original draft (supporting); Writing – review & editing (equal).

DATA AVAILABILITY

The data that support the findings of this study are available from the corresponding authors upon reasonable request.

REFERENCES

[1]H. Wang, Z. Li, X. Zhang, L. Zhu, Y. Liu, and S. Wang, "The motion of respiratory droplets produced by coughing," Phys. Fluids **32**(12), 125102 (2020).

[2]S. Feng and P. Wang, "The influences of boundary layer thickness on the characteristics of saltation sand flow—A large eddy simulation study," Aeolian Res. **60**, 100853 (2023).

[3]X. Zhang, B. Zhang, G. Xin, and G. Han, "The fluctuating characteristics of streamwise wind speed and total saltation mass flux in the near-neutral atmospheric surface layer," Phys. Fluids **35**, 026606 (2023).

[4]M. Chamecki and C. Meneveau, "Particle boundary layer above and downstream of an area source: Scaling, simulations, and pollen transport," J. Fluid Mech. **683**, 1–26 (2011).

[5]S. Balachandar and J. K. Eaton, "Turbulent dispersed multiphase flow," Annu. Rev. Fluid Mech. **42**, 111–133 (2010).

[6]L. Brandt and F. Coletti, "Particle-laden turbulence: Progress and perspectives," Annu. Rev. Fluid Mech. **54**, 159–189 (2022).

[7]G. H. Good, P. J. Ireland, G. P. Bewley, E. Bodenschatz, L. R. Collins, and Z. Warhaft, "Settling regimes of inertial particles in isotropic turbulence," J. Fluid Mech. **759**, R3 (2014).

[8]A. J. Petersen, L. Baker, and F. Coletti, "Experimental study of inertial particles clustering and settling in homogeneous turbulence," J. Fluid Mech. **864**, 925–970 (2019).

[9]H. Zhu, C. Pan, G. Wang, Y. Liang, X. Ji, and J. Wang, "Attached eddy-like particle clustering in a turbulent boundary layer under net sedimentation conditions," J. Fluid Mech. **920**, A53 (2021).

[10]D. O. Mora, M. Obligado, A. Aliseda, and A. Cartellier, "Effect of re_λ and rouse numbers on the settling of inertial droplets in homogeneous isotropic turbulence," Phys. Rev. Fluids **6**(4), 044305 (2021).

[11]M. R. Maxey, "The gravitational settling of aerosol particles in homogeneous turbulence and random flow fields," J. Fluid Mech. **174**, 441–465 (1987).

[12]X. Zheng, S. Feng, and P. Wang, "Modulation of turbulence by saltating particles on erodible bed surface," J. Fluid Mech. **918**, A16 (2021).

[13]J. Bec, H. Homann, and S. S. Ray, "Gravity-driven enhancement of heavy particle clustering in turbulent flow," Phys. Rev. Lett. **112**(18), 184501 (2014).

[14]K. O. Fong, O. Amili, and F. Coletti, "Velocity and spatial distribution of inertial particles in a turbulent channel flow," J. Fluid Mech. **872**, 367–406 (2019).

[15]C. Li, K. Lim, T. Berk, A. Abraham, M. Heisel, M. Guala, F. Coletti, and J. Hong, "Settling and clustering of snow particles in atmospheric turbulence," J. Fluid Mech. **912**, A49 (2021).

[16]L.-P. Wang and M. R. Maxey, "Settling velocity and concentration distribution of heavy particles in homogeneous isotropic turbulence," J. Fluid Mech. **256**, 27–68 (1993).

[17]B. Rosa, H. Parishani, O. Ayala, and L.-P. Wang, "Settling velocity of small inertial particles in homogeneous isotropic turbulence from high-resolution DNS," Int. J. Multiphase Flow **83**, 217–231 (2016).

[18]P. J. Ireland, A. D. Bragg, and L. R. Collins, "The effect of Reynolds number on inertial particle dynamics in isotropic turbulence. Part 2. Simulations with gravitational effects," J. Fluid Mech. **796**, 659–711 (2016).

[19]R. Monchaux and A. Dejoan, "Settling velocity and preferential concentration of heavy particles under two-way coupling effects in homogeneous turbulence," Phys. Rev. Fluids **2**(10), 104302 (2017).

[20]A. Aliseda, A. Cartellier, F. Hainaux, and J. C. Lasheras, "Effect of preferential concentration on the settling velocity of heavy particles in homogeneous isotropic turbulence," J. Fluid Mech. **468**, 77–105 (2002).

[21]P. Nielsen, "Turbulence effects on the settling of suspended particles," J. Sediment. Res. **63**(5), 835–838 (1993).

[22]T. S. Yang and S. S. Shy, "The settling velocity of heavy particles in an aqueous near-isotropic turbulence," Phys. Fluids **15**(4), 868–880 (2003).

[23]G. H. Good, S. Gerashchenko, and Z. Warhaft, "Intermittency and inertial particle entrainment at a turbulent interface: The effect of the large-scale eddies," J. Fluid Mech. **694**, 371–398 (2012).

[24]L. Baker, A. Frankel, A. Mani, and F. Coletti, "Coherent clusters of inertial particles in homogeneous turbulence," J. Fluid Mech. **833**, 364–398 (2017).

[25]T. Berk and F. Coletti, "Dynamics of small heavy particles in homogeneous turbulence: A Lagrangian experimental study," J. Fluid Mech. **917**, A47 (2021).

[26]C. Y. Yang and U. Lei, "The role of the turbulent scales in the settling velocity of heavy particles in homogeneous isotropic turbulence," J. Fluid Mech. **371**, 179–205 (1998).

[27]R. Monchaux, M. Bourgoin, and A. Cartellier, "Preferential concentration of heavy particles: A Voronoï analysis," Phys. Fluids **22**(10), 103304 (2010).

[28]H. Yoshimoto and S. Goto, "Self-similar clustering of inertial particles in homogeneous turbulence," J. Fluid Mech. **577**, 275–286 (2007).

[29]J. Tom and A. D. Bragg, "Multiscale preferential sweeping of particles settling in turbulence," J. Fluid Mech. **871**, 244–270 (2019).

[30]L. Pan, P. Padoan, and J. Scalo, "Turbulence-induced relative velocity of dust particles. II. The bidisperse case," Astrophys. J **791**(1), 48 (2014).

[31]R. Dhariwal and A. D. Bragg, "Small-scale dynamics of settling, bidisperse particles in turbulence," J. Fluid Mech. **839**, 594–620 (2018).

[32]H. Liu, Y. Feng, and X. Zheng, "Experimental investigation of the effects of particle near-wall motions on turbulence statistics in particle-laden flows," J. Fluid Mech. **943**, A8 (2022).

[33]Z. Zhu, R. Hu, Y. Lei, L. Shen, and X. Zheng, "Particle resolved simulation of sediment transport by a hybrid parallel approach," Int. J. Multiphase Flow **152**, 104072 (2022).

[34]A. Hammond and H. Meng, "Particle radial distribution function and relative velocity measurement in turbulence at small particle-pair separations," J. Fluid Mech. **921**, A16 (2021).

[35]A. D. Bragg, A. L. Hammond, R. Dhariwal, and H. Meng, "Hydrodynamic interactions and extreme particle clustering in turbulence," J. Fluid Mech. **933**, A31 (2022).

[36]H. Zhu, C. Pan, and H. Lian, "Spatial correlations and relative velocities of polydisperse droplets in homogeneous isotropic turbulence," Phys. Fluids **34**(8), 083320 (2022).

[37]G. Cui, I. Ruhman, and I. Jacobi, "Spatial detection and hierarchy analysis of large-scale particle clusters in wall-bounded turbulence," J. Fluid Mech. **942**, A52 (2022).

[38]H. Lian, G. Charalampous, and Y. Hardalupas, "Preferential concentration of poly-dispersed droplets in stationary isotropic turbulence," Exp. Fluids **54**(5), 1525 (2013).

[39]H.-Y. Zhu, C. Pan, J.-J. Wang, Y.-R. Liang, and X.-C. Ji, "Sand-turbulence interaction in a high-Reynolds-number turbulent boundary layer under net sedimentation conditions," Int. J. Multiphase Flow **119**, 56–71 (2019).

[40]H. Liu, X. He, and X. Zheng, "Amplitude modulation in particle-laden atmospheric surface layers," J. Fluid Mech. **957**, A14 (2023).

[41]N. Pandurangan and S. Sahu, "Spatial evolution of multi-scale droplet clusters in an evaporating spray," Phys. Fluids **34**, 113310 (2022).

[42]S. Elghobashi, "On predicting particle-laden turbulent flows," Appl. Sci. Res. **52**(4), 309–329 (1994).

[43]K. Ohmi and H.-Y. Li, "Particle-tracking velocimetry with new algorithms," Meas. Sci. Technol. **11**(6), 603 (2000).

[44]M. Manish and S. Sahu, "Analysis of droplet clustering in air-assist sprays using Voronoi tessellations," Phys. Fluids **30**, 123305 (2018).

[45]S. Sumbekova, A. Cartellier, A. Aliseda, and M. Bourgoin, "Preferential concentration of inertial sub-Kolmogorov particles: The roles of mass loading of particles, Stokes numbers, and Reynolds numbers," Phys. Rev. Fluids **2**(2), 024302 (2017).

[46]Y. Wang and K. M. Lam, "Clustering behaviour and settling velocity of bidisperse inertial particles in turbulent open channel flow," Int. J. Multiphase Flow **129**, 103303 (2020).

[47]M. Momenifar and A. D. Bragg, "Local analysis of the clustering, velocities, and accelerations of particles settling in turbulence," Phys. Rev. Fluids **5**(3), 034306 (2020).

[48]A. D. Bragg, P. J. Ireland, and L. R. Collins, "Mechanisms for the clustering of inertial particles in the inertial range of isotropic turbulence," Phys. Rev. E **92**(2), 023029 (2015).

[49]R. A. Shaw, "Particle-turbulence interactions in atmospheric clouds," Annu. Rev. Fluid Mech. **35**, 183–227 (2003).

[50]Z. Zhu, R. Hu, and X. Zheng, "A multiple-time-step integration algorithm for particle-resolved simulation with physical collision time," Int. J. Multiphase Flow **163**, 104411 (2023).

08 April 2024 03:27:00